AN EXPERIMENTAL INVESTIGATION OF DYNAMIC INELASTICITY AND FRACTURE OF NANOSTRUCTURED COATINGS

H. D. Espinosa, Z. Wu and B. C. Prorok

Department of Mechanical Engineering, Northwestern University
Evanston, IL 60208-3111, USA

ABSTRACT

The strength and ductility of nanocrystalline WC-Co cermets was evaluated with a modified Kolsky torsional bar. The test specimen structure consisted of a thin walled Al7075-T6 substrate 250 μm thick coated with a 250 μm thick WC-Co layer with an average grain size of 100 nm. Dynamic torsion tests indicated the coating strength to be ≅ 200 MPa. The coated specimens exhibited quasi-ductile behavior in that, after diffuse microcracking and failure of the coating, the aluminum substrate takes control of the post failure behavior.

The use of high-speed photography showed that damage to the coating occurred at the point where maximum load was attained. A sudden drop in load carrying capacity was observed when cracks coalesced into a well-defined fracture plane. This drop was immediately followed by load reduction governed by plastic deformation of the Al substrate

INTRODUCTION

WC-Co cermets are employed mainly as wear resistant materials. Properties of high hardness and toughness have encouraged their widespread use in a variety of applications, including mining, grinding, and metal cutting. Conventional grades of these cermets possess grain sizes in the 1-10 μm regime, with a morphology composed of a hexagonal WC phase bound together with a Co phase. Mechanical properties are significantly influenced by this microstructure in that hardness increases with grain size in accordance with the Hall-Petch relation [1,2].

Recent work has indeed demonstrated that nanostructured cermets offer improved mechanical properties over their coarse-grained counterparts [3]. Nanostructured materials are of great interest in systems where nano-grained morphology may improve the yieldability of what would otherwise be brittle materials. As a result they possess high interface-to-volume ratios that can expand plasticity and strain to failure of normally brittle materials [4,5]. Nanostructured materials can also exhibit increased hardness that follows the Hall-Petch relation to a critical point prior to saturation [6,7]. These benefits stem from the large number of nano-sized grains per unit volume and their accompanying large interface-to-volume ratio [5,8]. The presence of porosity in a nanostructured material can result in a lower than expected hardness and affects various other mechanical properties as well [9,10]. For the WC-Co cermet material, properties of increased hardness and enhanced strain to failure are very desirable. These advantages have been well documented for other submicrometer-grain-sized ceramics [11-14].

The wear resistant applications of WC-Co cermets inevitably expose them to mechanical conditions involving local dynamic loading and high strain rates. Testing of materials under such loading conditions present special challenges [15]. Dynamic fracture toughness can be evaluated by a number of techniques that include: Charpy test [16,17], drop-hammer experiment [18], and plate-impact experiment [19]. In employing these methods, the energy applied to the specimens is considerable, resulting in unstable growth upon crack initiation. Similarly, damage and inelasticity can be addressed using dynamic testing with specimen recovery [20-22]. A further consequence of these methods stems from computational and theoretical considerations that make up the basis for identifying damage initiation and evolution [23-24].

It is essential for present and future application design that we are able to predict the high strain rate response of the cermet material. With this in mind, a simple and accurate technique for studying dynamic loading conditions is the modified split Hopkins pressure bar [25]. This method has the advantage of loading the material under nearly uniform stress and strain rate. The integration of high-speed photography allows for the continual monitoring of specimen shape during testing. By this approach, a correlation can then be made between failure initiation and the stress-strain state of the specimen. This work investigates the response of WC-Co nanostructured materials under high strain rate conditions and examines the effect of loading rate on failure mode. It also evaluates the strength and ductility of the nano-grain sized coatings with unique instrumentation and specimen configuration.

EXPERIMENTAL PROCEDURE

Materials and processing

Nanocrystalline WC-Co coatings of 250 μm thickness were produced by a proprietary spraying process developed by A&A Company, Inc., South Plainfield, NJ. In this study, the alloy Al7075-T6 was machined as a thin-walled tube and used as the substrate. Both coated and uncoated aluminum specimens were tested to evaluate the mechanical properties of the nanocoatings. The geometrical dimensions of the WC-Co nano-coated samples used in the dynamic torsion test are given in Figure 1(a). The Young's modulus and Poisson's ratio of WC-Co and Al7075-T6 are: E_C = 520 GPa, ν_C = 0.28, and E_{Al} = 70.9 GPa, ν_{Al} = 0.36, respectively. Figure 1 shows micrographs of (b) micro-sized (3-4 μm) and (c) nano-sized (100 nm) grain structures. The micro-sized material provided a basis for comparison in the micro- and nano-indentation experiments. Both materials had the same 11 percent cobalt content. The surfaces of the coated specimens were painted with a very fine speckle pattern that was essential for imaging by high-speed photography and for strain analysis by digital speckle correlation. The ends of the sample were fixed to the incident and transmission bars by means of a high strength and fast curing adhesive (DEVCON 5 minute epoxy).

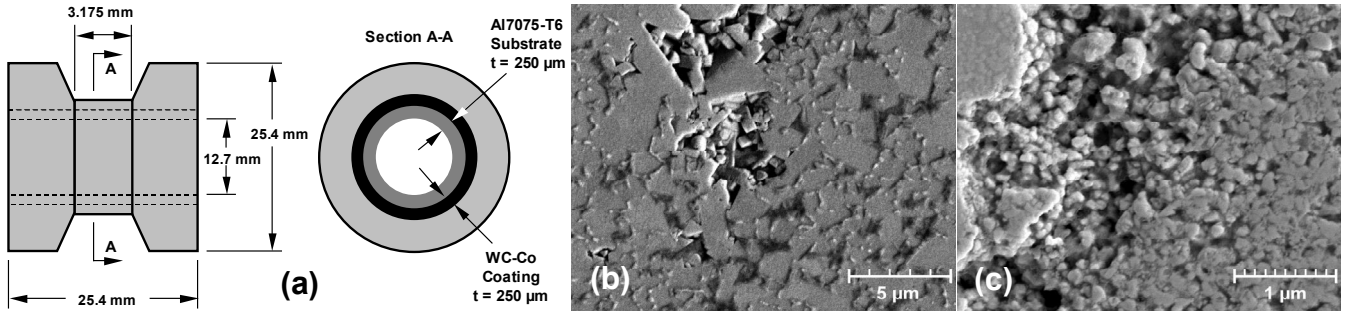

Figure 1: Schematic representation of WC-Co nanocrystalline coated dynamic torsion specimen (a). The dimensions of the Al7075-T6 substrate are identical for uncoated specimens. Photomicrograph of WC-Co (b) micro- and (c) nano-grain sized structures.

Mechanical testing

Our modified stored-energy Kolsky bar was used to obtain shear-stress / shear-strain curves at high strain rates [22,26,27]. The bar was integrated with a high-speed photography rig to observe deformation events and correlate them to specific points along the stress-strain curve.

High-speed photography

High-speed photography was used to independently monitor specimen inelasticity during testing. A Cordin Model 220-8 camera and K2 long distance microscope were used with a SUNPAK Auto 120J TTK high-power flash to acquire the images. Frames were captured at 20 μs intervals with exposure times of 1 μs. The incident pulse from the modified Kolsky bar was used to trigger the camera and flash.

Formulae

The functional dependence of strain rate on the incident, reflected, and transmitted shear strains for a single material specimen has been previously reported [28]. For a double-layered specimen, such as the WC-Co nano-coating on aluminum thin-walled substrate (see Figure 1(a)), the stresses and strains are obtained from the following equilibrium and compatibility relations:

$$T_T = G_{Al} \cdot I_{p,Al} \cdot \frac{\gamma_{Al}}{r_{Al}} + G_C \cdot I_{p,C} \cdot \frac{\gamma_C}{r_C} \quad , \quad \tau_{Al} = G_{Al} \cdot \gamma, \ \tau_C = G_C \cdot \gamma \tag{1}$$

$$\gamma_{Al} = \gamma_C = \frac{T_T}{G_{Al} \cdot 2\pi r_{Al}^2 t_{Al} + G_C \cdot 2\pi r_C^2 t_C} \tag{2}$$

where T_T is the transmitted torque, G is the shear modulus, I is the polar moment of inertia, γ is the shear strain, τ is the shear stress, r is the center line radius, and t is the shell thickness of the aluminum (AL) and of the coating (C). It is important to note that homogeneous deformation and compatibility in the double-layered specimens is violated when debonding at the aluminum-WC/Co interface or shear localization occurs.

RESULTS AND DISCUSSION

Dynamic Torsion

Shear stress – shear strain curves.

Three thin-walled sample configurations were selected for study. The first was an Al7075-T6 alloy thin-walled tube of thickness 250 μm coated with a 250 μm thick nanostructured WC-Co cermet. The second and third were uncoated Al7075-T6 thin-walled tubes of thickness 250 and 500 μm respectively, used comparatively for evaluating the nanocoatings mechanical properties.

The measured transmitted torque of the above samples is plotted as a function of time in Figure 2(a). For both uncoated Al7075-T6 specimens, (◇) denotes 250 μm thickness and (□) denotes 500 μm, the transmitted pulse has an extended steady state region at the top of the curve with large plastic deformations being recorded. However, for the WC-Co coated sample (◆), the transmitted pulse drops quickly after maximum transmitted torque is reached. This indicates that the WC-Co coating exhibits a quasi-brittle behavior and fractures at small inelastic deformations when compared to thin-walled Al7075-T6 specimens. The doubling of the wall thickness for the uncoated Al specimens translated into a doubling of the maximum transmitted torque as well as its steady state duration. The thin aluminum samples were found to be broken after the shear tests, a result of shear localization followed by fracture. This explains the reduction in transmitted pulse time to approximately one half of the pulse duration.

The WC-Co coating material is well bonded to the aluminum substrate. When this coating fails, the transmitted torque rapidly drops to a lower level before progressively decaying to zero. This indicates the inner-aluminum layer controls the post failure behavior. Furthermore, in view that the Young's modulus of WC-Co is much greater than that of Al7075-T6, the plastic deformation of the inner-aluminum layer is then constrained to a much narrower region. Thus, the total plastic deformation, on the whole specimen length, was smaller than in the case of the uncoated aluminum specimen. It can be expected that this sudden loss of load carrying capacity of the coating triggers shear localization in the aluminum substrate. This phenomenon was found to exist in all WC-Co nanocoated specimens subject to varying levels of incident

torque. Figure 2(b) is a plot showing transmitted torque signatures for specimens with incident torques of 200 Nm (●), 190 Nm (◆), 180 Nm (△), and 130 Nm (⊡). It should be noted that they are plotted on an arbitrary time scale to separate their signatures and that each data set lasted for a period of ≅ 250 μs. It is important to note that a higher incident torque did not always correspond to a higher transmitted torque. For example, the 180 Nm incident torque specimen exhibited the highest transmitted torque.

The shear stress and shear strain are easily obtained from the transmitted torque results via Eqs. (1) and (2). The shear stress and shear strain relationship that correspond to the experimental results in Figures 2(a) and 2(b) are plotted in Figures 2(c) and 2(d) respectively. Figure 2(c) compares the shear stress - shear strain relationship between the coated, (◆), and uncoated specimens, (◇) for 250 μm thickness and (□) for 500 μm. The 0.2 percent yield offset for both uncoated Al7075-T6 specimens was ≅ 185 MPa. The maximum shear stress was ≅ 220 MPa with corresponding shear strain of ≅ 20 percent and matches well with those reported in the literature. The results for the thin- and thick-walled samples are almost identical with exception to an extended plastic zone and a sharper decrease in shear stress toward failure.

For the coated specimen (◆), the maximum shear stress was ≅ 200 MPa. The abrupt drop after attaining maximum shear stress indicated that micro-cracking began with the offset of yielding by the substrate. As observed in the transmitted torque results discussed earlier, following the sudden drop in shear stress, the average plasticity leveled off and progressively decayed to complete failure. This is a clear indication that the inner-aluminum layer controls the post failure behavior.

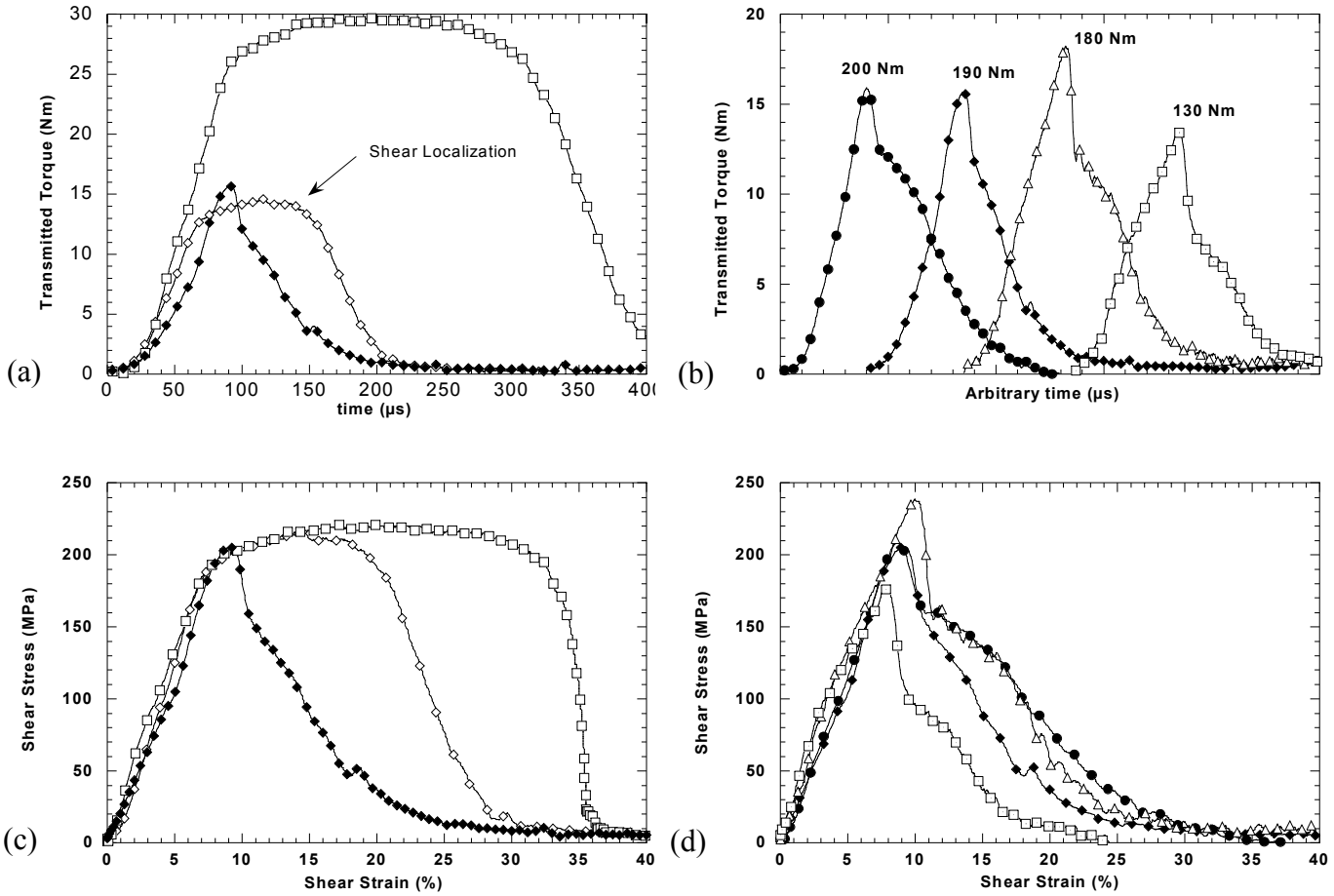

Figure 2: Transmitted torque-time signatures, (a) and (b), and the calculated shear stress - shear strain signatures, (c) and (d). Where (◆) denotes the nanocoated specimen, (◇) and (□) demote the uncoated Al7075-T6 thin-walled tubes of thickness 250 μm and 500 μm respectively, and various incident torques of nanocoated specimens are; 200 Nm (●), 190 Nm (◆), 180 Nm (△), and 130 Nm (⊡).

This transition in failure behavior was also observed in all coated samples with varying applied incident torque, Figure 2(d). In these data, the maximum shear stress attained for the coated specimens was ≅ 200 ± 30 MPa, reaching a maximum when the incident torque was 180 Nm. The absence of an extended strain to

failure region in the stress-strain curve for the nanocoated specimens is likely the result of extensive porosity in the coating material. This aspect was identified in the hardness discussion above.

The hardness of the micro- and nano-grain sized WC-Co was evaluated and revealed that hardness remained relatively uniform in the micro-indentation regime for both grain-size structures yielding values between 12–13 GPa. Nano-indentation revealed a significant change in behavior where the micro-sized material exhibited an increase in hardness to ≅ 20 GPa while the nano-sized material first showed hardness to be equivalent to the micro-indentation data at a depth of 500 nm and then increased to ≅ 20 GPa at a depth of 200 nm. Given the degree of coating porosity of the nano-sized material, the microstructure consists of hard agglomerates (clusters of nano-sized crystals strongly bonged together) that likely behave in a manner similar to the micro-grained material during the indentation tests.

High-speed photography.
Figure 3(a) is a series of images showing the surface of the coated thin-walled specimen. This series depicts a time sequence during torsional loading where a speckle pattern applied to the surface is used to determine the relative shear deformation experienced by the specimen. Two areas of the surface are denoted with a square (A) and a circle (B) that track the movement of specific speckles relative to each other. For the specimen in Fig. 9, the position of square A does not significantly change during the test. However, circle B was observed to displace continuously over time as a result of coating cracking and shear localization. After 70 μs circle B moved 21.2 μm relative to square A, resulting in an average shear strain of 2.85 percent. After 90μs the displacement increased to 105.8 μm and the average shear strain increased to 14.2 percent. There is also the initiation of a crack denoted by the arrow. Displacement and average shear strain increased with time until failure. These strains are a localized examination and differ from those calculated in Figure 2 under the homogeneous deformation assumption.

Synchronization of strain analysis and high-speed photography.
The data from dynamic torsion testing can be synchronized with the frames obtained from high-speed photography by matching their time scales. Figure 3(b) is a plot of the transmitted torque versus time for the coated specimen. Superimposed on this plot are the time markers for when each frame of Figure 3(a) was acquired during the test. Frames 1 (0 μs) and 2 (70 μs) were captured before the maximum transmitted torque was attained. When the microcracks coalesce into a dominant crack the coating fails and the aluminum substrate then governs the deformation behavior until failure.

CONCLUSIONS

Specialized equipment and specimens were developed to investigate strength and ductility of nanocrystalline WC-Co coatings. Dynamic torsion experiments with well-defined stress pulses were performed. These experiments revealed that the strength of WC-12%Co cermets, with an average grain size of about 100 nm, was about 200 MPa. The coating exhibits a quasi-ductile behavior as observed in deformation patterns. High-speed photography carried on in real time showed that coating damage occurred in the vicinity of the stress peak. Furthermore, the images revealed that a sudden drop in load carrying capacity coincides with micro-crack coalescence leading to the formation of a well-defined fracture plane in the coating. The stress peak in the coated material also coincides with the onset of large plastic deformation of the aluminum substrate. It is likely that shear localization in the aluminum thin-walled specimen is triggered by fracture of the coating and subsequently confined to the narrow region of the failed coating. The end result is the overall splitting of the specimen in two pieces.

Although the properties of the WC-Co nano-coating were far from optimum, a new methodology for investigating failure has been established. This methodology can be applied to examine the behavior of other advanced materials that can be manufactured as coatings on ductile substrates.

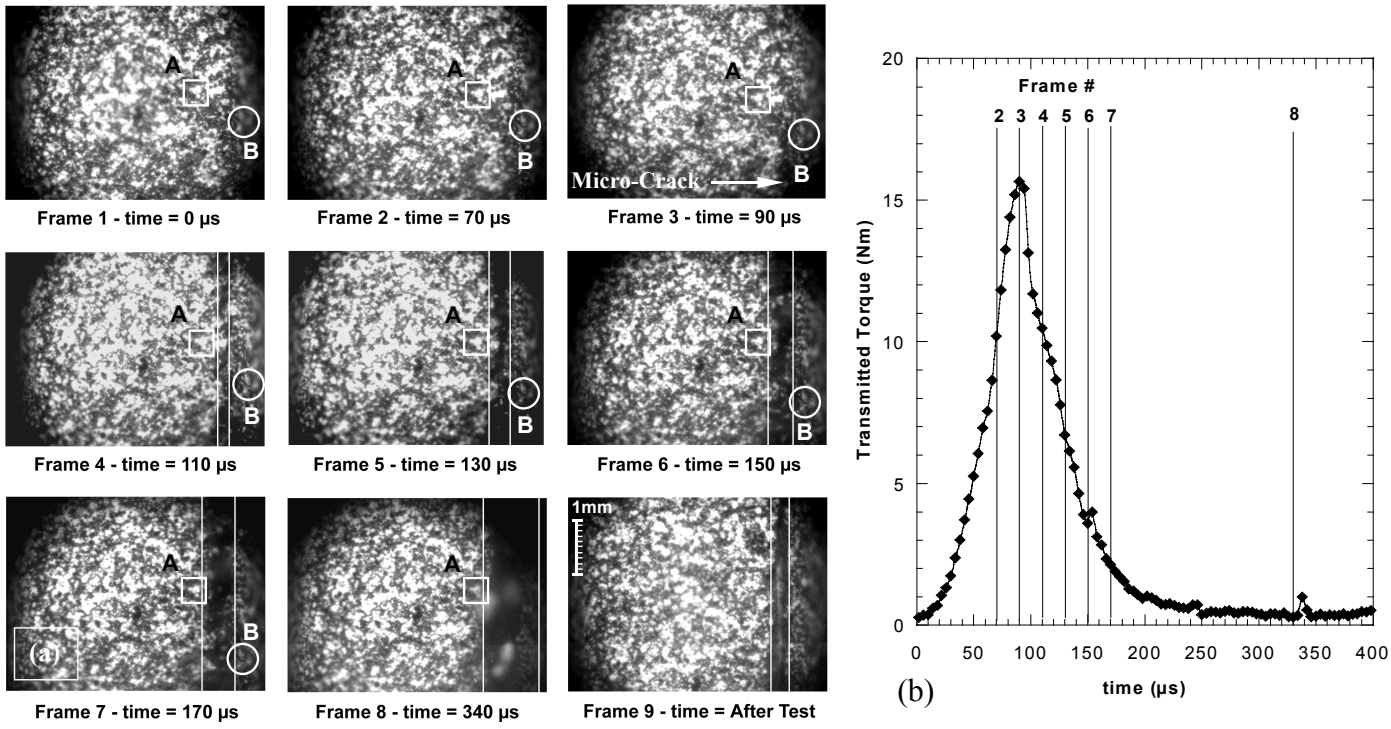

Figure 3: (a) High speed photography images taken during a dynamic shear test and (b) synchronization of frames with dynamic strain analysis data (b).

REFERENCES

1 Halls, E.O. (1951), *Proc. Phys. Soc. Lond.*, B64, 747.
2 Petch, N.J. (1953), *J. Iron Steel Inst.*, 174, 25.
3 Zhang, Z., Wahlberg, S., Wang, M., and Muhammad, M. (1999), *Nanostruc. Mater.*, 12, 163.
4 Kung, H. and Foecke, T., *ibid.*, 14.
5 Weertman, J.R., Farkas, D., Hemker, K., Kung, H., Mayo, M., Mitra, R., and van Swygenhoven, H. (1999), *MRS Bulletin*, 24(2), 44.
6 Nieh, T. G. and Wadsworth, J. (1991), *Scripta Metall. Mater.*, 25, 955.
7 Scattergood, R.O. and Koch, C.C. (1992), *ibid.*, 27, 1195.
8 Coble, R.L. (1965), *J. Appl. Phys.*, 34, 1679.
9 Mayo, M.J., Siegel, R.W., Narayamy, A., and Nix, W.D. (1990), *J. Mater. Res.*, 5, 973.
10 Mayo, M.J., Siegel, R.W., Liao, Y.X., and Nix, W.D. (1992), *ibid.*, 7, 1073.
11 Nieh, T.G., McNally, C.M., and Wadsworth, J. (1989), *J. Met.*, 31.
12 Maehara, Y. and Langdon, T.G. (1990), *J. Mater. Sci.*, 25, 2275.
13 Nieh, T.G., Wadsworth, J., and Wakai, F. (1991), *Int. Mater. Rev.*, 36, 146.
14 Mayo, M.J. (1997), *Nanostruc. Mater.*, 9, 717.
15 Espinosa, H.D. and Nemat-Nasser, S. (2000), *ASM Handbook, Mech. Testing and Evaluation*, 8.
16 Ruiz, C. and Mines, R.A.W. (1985), *Int. J. Fracture*, 29, 101.
17 Kobayashi, T., Yamamoto, I., and Niinomi, M. (1986), *Engineering Fracture Mechanics*, 24, 773.
18 Eftis, J. and Krafft, J.M. (1965), *J. of Basic Engineering, Trans. ASME*, 257, 89.
19 Prakash, V. and Clifton, R. (1993), *Trans. ASME*, 165, 412.
20 Subbash, G. and Ravichandran, G. (2000), *ASM Handbook, Mechanical Testing and Evaluation*, 8.
21 Nemat-Nasser, S., *ibid*.
22 Espinosa, H.D., Patanella, A., and Xu, Y. (2000), *Exp. Mech.*, 40(3), 1.
23 Espinosa, H.D., Zavattieri, P.D., and Dwivedi, S. (1998), *J. Mech. and Phy. of Sol.*, 46(10), 1909.
24 Zavattieri, P.D., Raghuram, P., and Espinosa, H.D. (2000), *J. Mech. and Phy. of Sol.*, 49, 27.
25 Kolsky, H. (1949), *Proc. Phys. Soc. Lon.*, B62, 676.
26 Espinosa, H.D., Patanella, A., and Fischer, M. (2000), *J. Tribology*, 122, 1.
27 Ibid. (2000), *Exp. Mech.*, 40(2), 138.
28 Meyers, M.A. (1994), *Dynamic Behavior of Materials*, John Wiley & Sons Inc., New York, 305.